Nanoscale Res Lett (2008) 3:65–70
DOI 10.1007/s11671-008-9117-5

NANO EXPRESS

Iron Oxide Nanoparticles Employed as Seeds for the Induction of Microcrystalline Diamond Synthesis

Kishore Uppireddi · Oscar Resto · Brad R. Weiner · Gerardo Morell

Received: 3 October 2007 / Accepted: 9 January 2008 / Published online: 24 January 2008

Abstract Iron nanoparticles were employed to induce the synthesis of diamond on molybdenum, silicon, and quartz substrates. Diamond films were grown using conventional conditions for diamond synthesis by hot filament chemical vapor deposition, except that dispersed iron oxide nanoparticles replaced the seeding. X-ray diffraction, visible, and ultraviolet Raman Spectroscopy, energy-filtered transmission electron microscopy , electron energy-loss spectroscopy, and X-ray photoelectron spectroscopy (XPS) were employed to study the carbon bonding nature of the films and to analyze the carbon clustering around the seed nanoparticles leading to diamond synthesis. The results indicate that iron oxide nanoparticles lose the O atoms, becoming thus active C traps that induce the formation of a dense region of trigonally and tetrahedrally bonded carbon around them with the ensuing precipitation of diamond-type bonds that develop into microcrystalline diamond films under chemical vapor deposition conditions. This approach to diamond induction can be combined with dip pen nanolithography for the selective deposition of diamond and diamond patterning while avoiding surface damage associated to diamond-seeding methods.

K. Uppireddi (✉) · B. R. Weiner · G. Morell
Institute for Functional Nanomaterials, University of Puerto Rico, San Juan, PR 00931, USA
e-mail: uppireddi@gmail.com

K. Uppireddi · O. Resto · G. Morell
Department of Physics, University of Puerto Rico, San Juan, PR 00931, USA

B. R. Weiner
Department of Chemistry, University of Puerto Rico, San Juan, PR 00931, USA

Keywords Iron nanoparticle · Diamond · EFTEM · EELS · Dip pen nanolithography

Introduction

Many challenges remain opening regarding the integration of diamond into electronic devices. In particular, seeding processes are typically harsh on the substrate surface, leading to defect creation and lack of reproducibility. Iron-based materials have been used as catalysts in the synthesis of crystalline diamond by high temperature, high-pressure growth [1–3]. Yet, it is difficult to fabricate diamond on iron-based materials by chemical vapor deposition (CVD) due to the rapid diffusion of carbon into the bulk and high carbon solubility [4]. There have been a number of attempts to grow diamond by forming a thin film of iron on silicon substrates [5–7]. Higher diamond nucleation densities with significant amounts of a–C are attained by depositing a thin layer of iron on silicon substrates, thus suggesting that a high carbon concentration resulting in a saturated carbide layer during the initial stage of nucleation is required for producing diamond nucleation sites [8, 9]. Reports by Ahn et al. [10] and Kohmura et al. [11] further indicate that there is an optimum iron thickness at which diamond growth prevails.

The above-described developments suggest that the Fe nanoparticles can be employed as diamond nucleation centers: they have a strong affinity for C atoms and yet they are too small to act as C sinks. FeO nanoparticles (nFeO) are ideal candidates for this task because the Fe nanoparticle is passivated by O, which is then removed by the CVD reactions, leaving the active Fe nanoparticle exposed for C trapping and accumulation. The results hereby reported evidence the success of this approach.

Experimental Details

Microcrystalline diamond particles and films were synthesized using a custom-built hot filament CVD (HFCVD) apparatus, which is described in detail elsewhere [12]. The films were grown on 14-mm diameter and 0.5-mm thick Mo, Si, and quartz substrates. The substrates were cleaned by sonication in methanol and acetone and dried with inert gas. After cleaning, a suspension of nFeO with nominal particle size distribution in the 7–10 nm range (Integran Technologies Inc.) was applied to the substrates. The surface density of nFeO clusters was estimated to be $\sim 10^7$ cm^{-2} by atomic force microscopy and scanning electron microscopy (SEM). However, scattered micron-size patches of unseeded substrate remained. No diamond powder seeding was employed.

A mixture of 2% CH_4 in H_2 with a total flow of 100 sccm was directed over the heated rhenium filament kept at 2,700 K and 10 mm above the substrate. The total pressure was kept constant at values between 20 and 50 Torr (2.6–6.6 kPa). The substrates were maintained around 700–730 °C and the deposition time was varied between 30 min and 6 h.

The surface morphology of the films was investigated by SEM using a JEOL JSM 845A Model microscope. Small portions of the diamond samples were placed on Formvar-coated Cu grids and uncoated silicon nitride TEM grids for energy-filtered transmission electron microscopy (EFTEM) and electron energy-loss spectroscopy (EELS) using an energy-filtered LEO 922 OMEGA microscope operating at an accelerating voltage of 200 kV. The structural phases of the films were characterized by micro-Raman spectroscopy (RS) using a triple monochromator (ISA Jobin-Yvon Inc. Model T64000) with 1 cm^{-1} resolution and the 514.5 nm Ar-ion laser line for excitation. The spectra were recorded using an 80× objective that probes an area of about 1–2 μm^2. The UV Raman spectra were measured using a double monochormator (ISA Jobin-Yvon Inc.) with a resolution of 3–4 cm^{-1} and the second harmonic generation of 488 nm radiation (244 nm) from an Ar-ion laser.

The X-ray diffraction (XRD) measurements were taken on a Siemens D5000 diffractometer using the Cu K_α line source ($\lambda = 1.5405$ Å) in θ–2θ configuration. The X-ray photoelectron spectroscopy (XPS) measurements were taken using a Physical Electronic system (Model PHI5600 ESCA, MN, USA) for elemental analysis at room temperature, which was operated in the constant energy pass mode using monochromatic Al K_α X-rays ($h\upsilon = 1{,}486.6$ eV). The resolution of the electron energy analyzer was around 0.25 eV.

Results and Discussion

The structure of the initial nFeO was determined by XRD (Fig. 1a). The diffractogram corresponds to cubic iron oxide (i.e., maghemite). The average size of the nanoparticles was determined to be around 10 nm using EFTEM (Fig. 1b). These nFeO induced the synthesis of microcrystalline diamond, as shown in the SEM images of Fig. 2 for different deposition times: 0.5, 2, and 6 h. Micron-size well-faceted diamond particles are readily observed for a deposition time of 30 min, as shown in Fig. 2a. The diamond crystallite size increased proportionally for a deposition time of 2 h, and lateral collision of growing particles began forming a film, as shown in Fig. 2b. A deposition time of 6 h led to quite continuous films of about 10–11 μm thickness with a few scattered gaps, as shown in Fig. 2c. The Bragg reflections characteristic of ⟨111⟩ and ⟨400⟩ diamond lattice planes were obtained for all the films (data not shown). Control experiments to grow diamond directly on Mo, Si, and quartz without nFeO or diamond seeding were unsuccessful for deposition times of 6 h, as expected, except for the formation of a MoC or a SiC surface layer according to XRD [13].

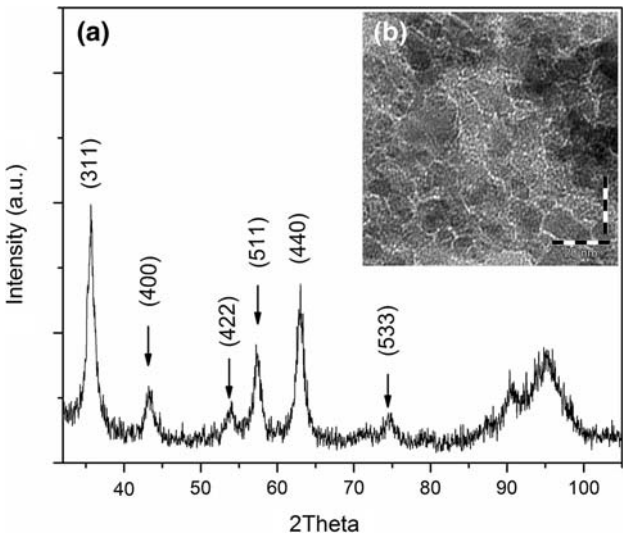

Fig. 1 (**a**) X-ray diffractogram of nFeO particles employed to induce diamond growth. The peaks labeled correspond to cubic FeO crystal structure. (**b**) EFTEM image of nFeO showing its particle size in the range of 7–10 nm

The diamond growth rates were around 1.7–1.9 μm/h, which is substantially high for HFCVD (typically 0.1–0.2 μm/h), and the observed nucleation densities were around 10^7 cm^{-2}, corresponding well to the initial nFeO density and similar to those typically obtained by diamond-seeded diamond deposition [14]. In contrast, previous reports of methods involving some form of Fe seeding, typically thin Fe films, suffered from low growth rates and substantial co-deposition of amorphous carbon (a–C) [6, 7]. Although there might be a slight effect on the nucleation density due to mechanical polishing of the Mo substrates [15], it does not sufficient to account for the results

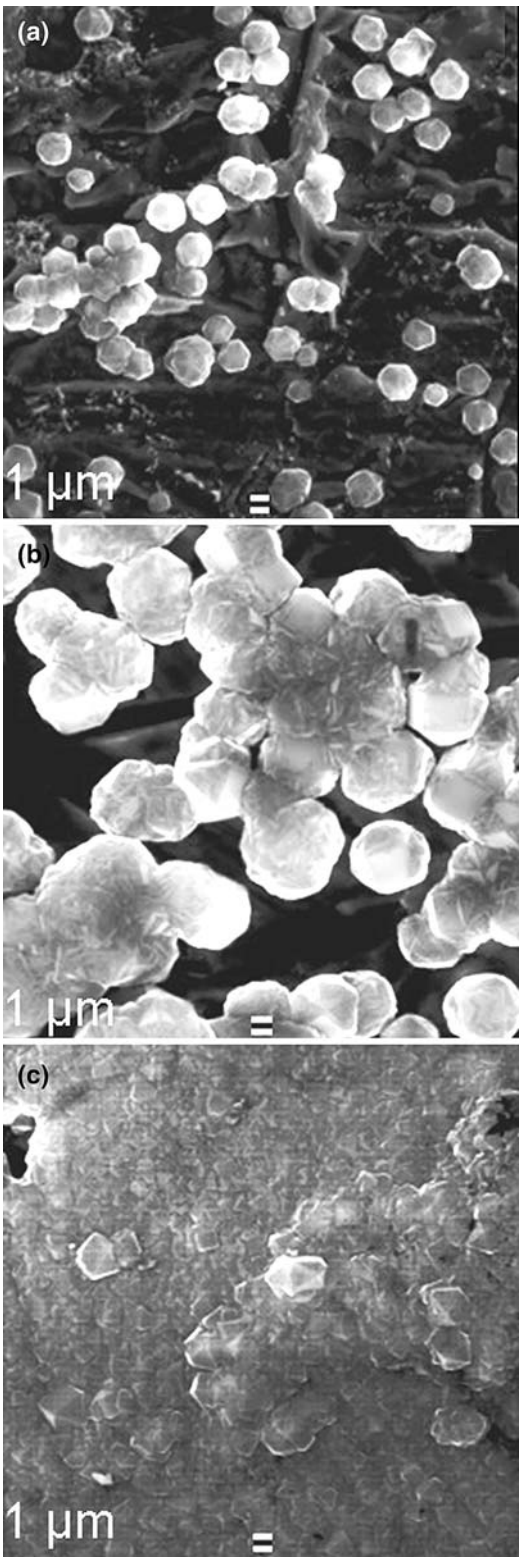

Fig. 2 SEM images of nFeO-induced diamond deposited on Mo substrates for: (**a**) 30 min, (**b**) 2 h, and (**c**) 6 h

described above, especially since the quartz and Si substrates were not mechanically polished but nevertheless the growth of a microcrystalline diamond film was also successfully induced on them by nFeO. Another important difference is the diamond quality of the nFeO-induced diamond films according to their Raman spectra.

The bonding structure of the material was determined by RS excited with two radiation energies: visible (2.4 eV) and UV (5.1 eV). The combination of visible and UV Raman is an effective approach for probing both kinds of carbon materials because the Raman scattering cross-section for sp^2-bonded carbon in the visible region is 50–230 times higher than that of sp^3-bonded carbon [16]. The Stokes-shifted visible and UV Raman spectra of the nFeO-induced diamond films are shown in Fig. 3a. They indicate that there is a relatively small presence of sp^2-bonded carbon in the nFeO-induced diamond films. (No plasma etching or any other treatment was performed to enhance the post-deposition diamond quality of the films.)

The deconvolution of the Raman spectra was done using a Voigt function corresponding to the diamond peak, and five Gaussians corresponding to the D and G bands, and the bands centered at $\sim$1,285, 1,490, and 1,610 cm^{-1} [17–19]. The spectra were corrected for instrumental broadening to obtain the intrinsic diamond peak widths [20, 21]. Figure 3b shows a sample spectral simulation. The diamond peak FWHM obtained from these simulations is $\sim$8–10 cm^{-1}, and the diamond quality factor is around 97–98%, further indicating the good quality of the films and their similarity to diamond-seeded HFCVD diamond films. The diamond peak is always blue-shifted in the 1,333.5–1,335.5 cm^{-1} range, indicating compressive stresses of around 0.6–1.7 GPa. Similar Raman spectra, growth rates, XRD diffractograms are obtained for nFeO-induced diamond films deposited on quartz, Si, and Mo substrates under identical conditions, thus confirming the consistency of the above-described results and ruling out the possibility of an underlying substrate effect.

Energy-filtered transmission electron microscopy and EELS were employed to investigate the initial growth phase of nFeO-induced diamond [22]. The high-resolution EFTEM image shown in Fig. 4 shows the aggregation of carbon and formation of lattice planes around a seed nanoparticle (dark region). A fast Fourier transform analysis was employed to measure the spacing between the atomic planes, which were found to vary. The lattice spacing in different regions was measured to be 1.1, 1.16, 1.24, and 3.33 ± 0.1 Å. These values correspond to graphite $\langle 006 \rangle$, $\langle 112 \rangle$, $\langle 110 \rangle$, and $\langle 002 \rangle$ interplanar spacing, respectively, and at the same time the 1.1 and 1.24 ± 0.1 Å values also correspond to diamond $\langle 311 \rangle$ and $\langle 220 \rangle$ interplanar spacing, respectively. Taken altogether, these results point toward the aggregation of graphitic carbon around the seed nanoparticle and the impending formation of diamond.

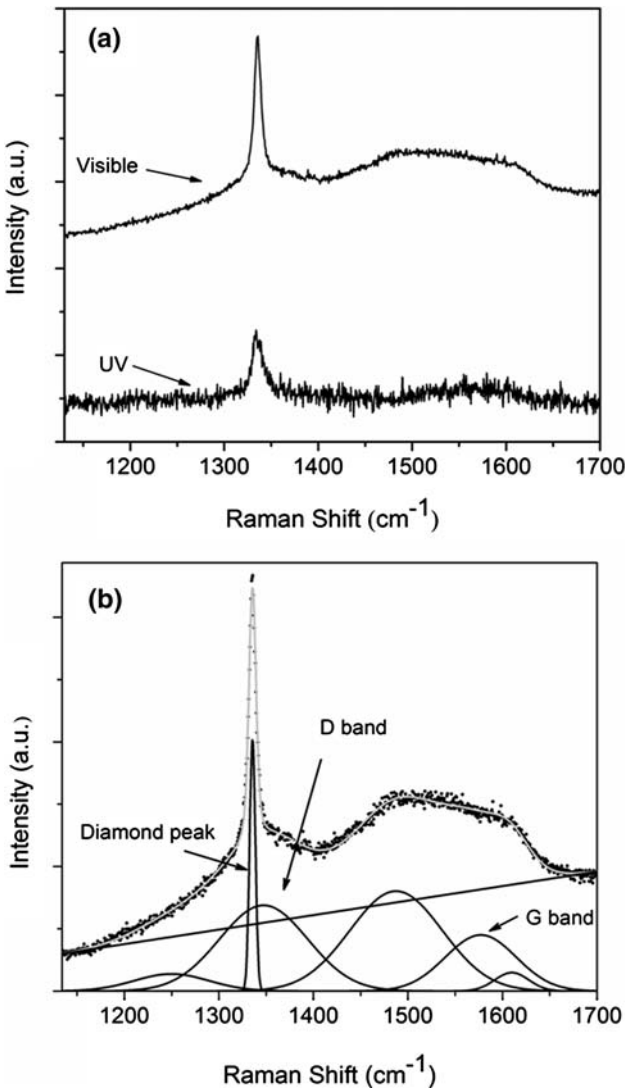

Fig. 3 (**a**) Representative visible and UV Raman spectra of nFeO-induced microcrystalline diamond on Mo substrates. (**b**) Deconvoluted visible Raman spectrum, showing the diamond peak with FWHM of 9 cm^{-1} and peak position at 1,335 cm^{-1}

Parallel EELS core-loss spectra of carbon K-edge and iron L-edge were collected on the area as shown in Fig. 4, and the corresponding spectra for nFeO, a–C, and diamond were also obtained for comparison [23, 24], as shown in Fig. 5. There are features at ~285, ~290, ~297, ~305, and ~325 eV in the carbon K-edge spectrum. The peak at ~285 eV corresponds to the $0 \rightarrow \pi^*$ electronic transition and is thus a signature of sp^2-bonded carbon [25]. The higher energy features correspond to $0 \rightarrow \sigma^*$ transitions of diamond-type carbon bonds [23, 26]. The observed broadening and smoothening of the EELS features corresponding to diamond-type bonds is due their co–existence with trigonally bonded carbon in the near-seed region. The Fe 2p edge shows a peak at ~710 eV (Fig. 5b), corresponding to the due to transition of electrons from 2p orbitals to unoccupied 3d

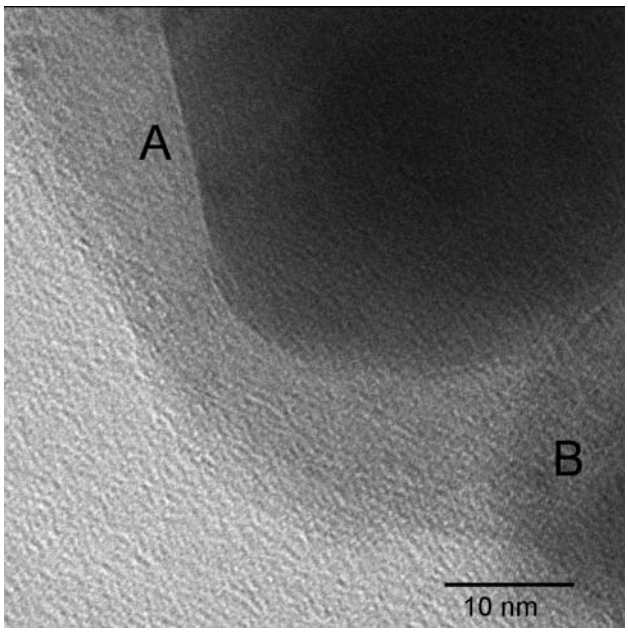

Fig. 4 EFTEM image showing the aggregation of carbon material around the Fe nanoparticle (dark area). The zones of EELS analyses are labeled as A and B

orbitals [24], confirming the role of iron nanoparticles as carbon clustering centers. No oxygen signal was detected by EELS due to the fact that the HFCVD conditions promote the reaction of surface O with H and C atoms to form HO and CO radicals, thus leaving the bare iron particles available to act as C traps.

We also studied the average bonding environment of the material by XPS. The carbon 1s core spectrum (Fig. 6) indicates the strong presence of tetrahedral carbon (sp^3 C) [27], in agreement with the Raman spectra. It also shows a strong oxygen 1s signature and a weak iron 2p signature at 531.5 and 711 eV, respectively [28, 29]. The presence of O on the surface is due to post-deposition adsorbates, while the relatively small Fe signature further confirms its saturation with C.

It has been reported that the formation of a very dense amorphous carbon phase can lead to diamond nucleation [30–32]. In this process, sp^3-bonded C clusters start precipitating by consuming the carbon atoms from the dense amorphous carbon phase. Furthermore, there are theoretical studies indicating that diamond nuclei are stable structures when embedded in a–C matrix [33], and experiments showed that these serve as nucleation centers for subsequent growth [31]. Thus the formation of a dense amorphous carbon phase is a plausible route for nucleating diamond. The iron nanoparticle may act as catalyst in decomposing the hydrocarbon under CVD conditions, after oxygen removal from the initial nFeO, leading to active carbon adsorption [34, 35]. Since there is no room for diffusion into the interior of the Fe nanoparticle and the

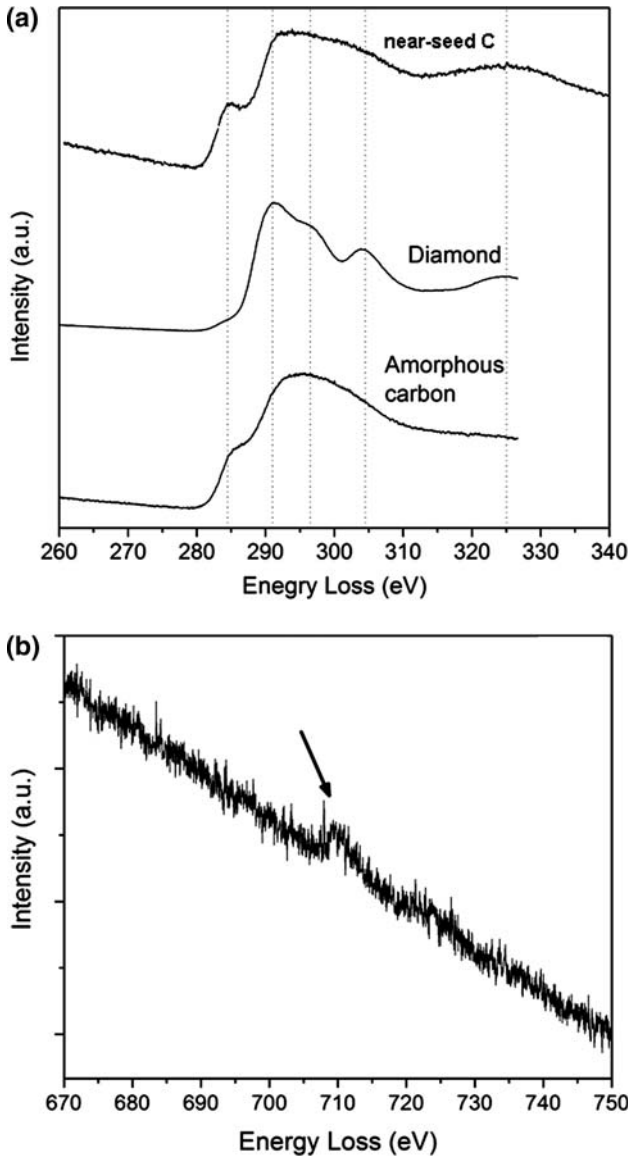

Fig. 5 (**a**) Carbon K-edge EELS obtained from the edge of the dark area (location B in Fig. 4), indicating the presence of sp^2 and sp^3 bonding along with the corresponding reference data for diamond and amorphous carbon. The dashed lines indicate the positions of peaks and shoulders as discussed in the text. (**b**) Iron L-edge of the same area (location B in Fig. 4) showing the presence of iron L_3 ($2P_{3/2}$) transition

amount of carbon that the Fe nanoparticle can adsorb is limited, there occurs densification of trigonally and tetrahedrally bonded carbon around the iron nanoparticle and the impending formation of diamond bonds.

From the above analysis, the synthesis of nFeO-induced microcrystalline diamond films can be summarized as follows: (a) iron oxide nanoparticles lose oxygen by chemical vapor reactions that lead to the formation HO and CO radicals, creating active nanoscale iron surfaces for the adsorption and decomposition of the incoming carbon-containing species, and thus for the formation of nanoscale

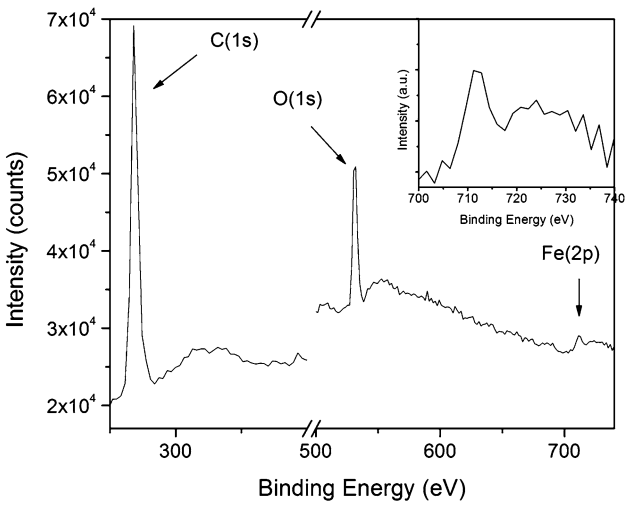

Fig. 6 XPS spectra of nFeO-induced diamond showing the carbon 1s, oxygen 2p, and iron 2p peaks. The inset shows the enlarged iron 2p peak

C clusters with trigonal and tetrahedral C bonds; (b) as these carbon clusters densify around the iron nanoparticles, diamond-type bonds start precipitating [30]; and (c) diamond film deposition continues to occur under conventional diamond growth conditions of high hydrogen dilution which keep the growing surface hydrogenated and preferentially etch away the trigonal carbon bonds.

Conclusions

The iron oxide nanoparticles were employed to induce the formation of diamond nuclei and the synthesis of microcrystalline diamond films. This approach yields relatively high diamond growth rates, low presence of amorphous carbon and can be used for the selective diamond deposition and patterning at the nanoscale through dip pen nanolithography of nFeO followed by chemical vapor deposition. The combined analysis of the various characterization results, indicate that the iron nanoparticles act as nucleation and aggregation sites for carbon and the impending formation of diamond-type bonds. The formation of a dense, mixed C phase around the Fe nanoparticles leading to the precipitation of sp^3 C bonds is proposed as a plausible explanation for these results.

Acknowledgments One of the authors (K.U.) acknowledges the Graduate Research Fellowship granted by the National Science Foundation (Grant No. EPS-0223152). This research project is being carried out under the auspices of the Institute for Functional Nanomaterials (NSF Grant No. 0701525). This research was also supported in parts by NASA Training Grant NNG05GG78H (PR Space Grant), NASA Cooperative Agreement NCC5-595 (PR NASA EPSCoR), and NASA Grant NCC3-1034 (NASA CNM URC). We gratefully acknowledge the use of research facilities of Dr. R. Katiyar,

Mr. W. Pérez (micro-Raman spectroscopy), Dr. Antonio Martínez, Mr. Javier Wu (SEM), Dr. Carlos Cabrera (XPS), Ms. Lyda La Torre, and Dr. Vladimir Makarov, Dr. Fabrice Piazza for their discussions.

References

1. F.P. Bundy, H.P. Bovenkerk, H.M. Strong, R.H. Wentorf Jr, J. Chem. Phys. **35**, 383 (1961)
2. B.V. Deryaguin, L.L. Builov, V.M. Zubkov, A.A. Kochegina, D.V. Fedoseev, Sov. Phys. Crystallogr. **14**, 449 (1969)
3. K.E. Spear, J.P. Dismukes, *Synthetic Diamond: Emerging CVD Science and Technology* (Wiley, New York, 1994)
4. T. Sato, S. Narumi, S. Ito, K. Akashi, Thin Solid Films **316**, 29 (1998)
5. K. Kobayashi, N. Mutsukura, Y. Machi, T. Nakano, Diamond Realt. Mater. **2**, 278 (1993)
6. Y. Shimada, N. Mutsukura, Y. Machi, Diamond Realt. Mater. **2**, 656 (1993)
7. Y. Shimada, Y. Machi, Diamond Realt. Mater. **3**, 403 (1994)
8. Y. Machi, New Technol. Jpn **19**, 913 (1991)
9. V.P. Godbole, J. Narayan, J. Appl. Phys. **71**, 4944 (1992)
10. J. Ahn, F.H. Tan, H.S. Tan, Diamond Relat. Mater. **2**, 353 (1992)
11. N. Kohmura, K. Sudoh, K. Sato, K.K. Hirakuri, K. Miyaka, G. Friedbacher, Diamond Realt. Mater. **14**, 283 (2005)
12. G. Morell, E. Canales, B.R. Weiner, Diamond Relat. Mater. **8**, 166 (1999)
13. S. Gupta, G. Morell, R.S. Katiyar, D.R. Gilbert, R.K. Singh, Diamond Relat. Mater. **8**, 185 (1999)
14. S. Gupta, B.R. Weiner, G. Morell, J. Mater. Res. **17**, 1820 (2002)
15. J.C. Arnault, L. Demuynck, C. Speisser, F. Le Normand, Eur. Phys. J. B **11**, 327 (1999)
16. J. Wagner, C. Wild, P. Koidl, Appl. Phys. Lett. **59**, 779 (1991)
17. F. Tuinstra, J.L. Koenig, J. Chem. Phys. **53**, 1126 (1970)
18. A.C. Ferrari, J. Robertson, Phys. Rev. B **63**, 121405 (2001)
19. F. Piazza, J.A. González, R. Velázquez, J. De Jesús, S.A. Rosario, G. Morell, Diamond Relat. Mater. **15**, 109 (2006)
20. G. Morell, W. Perez, E. Ching-Prado, R.S. Katiyar, Phys. Rev. B **53**, 5388 (1996)
21. G. Morell, O. Quiñones, Y. Díaz, I.M. Vargas, B.R. Weiner, R.S. Katiyar, Diamond Relat. Mater. **7**, 1029 (1998)
22. R.F. Egerton, *Electron Energy-Loss Spectroscopy in the Electron Microscopy* (Plenum, New York, 1996)
23. D.M. Gruen, Annu. Rev. Mater. Sci. **29**, 211 (1999)
24. L.A.J. Garvie, A.J. Craven, R. Brydson, Am. Mineral. **79**, 411 (1994)
25. P.J. Fallon, L.M. Brown, Diamond Relat. Mater. **2**, 1004 (1993)
26. C. Popov, W. Kulisch, S. Boycheva, K. Yamamoto, G. Ceccone, Y. Koga, Diamond Relat. Mater. **13**, 2071 (2004)
27. D.N. Belton, S.J. Harris, S.J. Schmieg, A.M. Weiner, T.A. Perry, Appl. Phys. Lett. **54**, 416 (1989)
28. A.J. McEvoy, W. Gissler, Thin Solid Films **83**, L165 (1981)
29. J. Schwar, P.W. John, L. Wiedmann, A. Benninghoven, J. Vac. Sci. Technol. A **9**, 238 (1991)
30. Y. Yao, M.Y. Liao, Z.G. Wang, Y. Lifshitz, S.T. Lee, Appl. Phys. Lett. **87**, 063103 (2005)
31. W.J. Zhang, X.S. Sun, H.Y. Peng, N. Wang, C.S. Lee, I. Bello, S.T. Lee, Phys. Rev. B **61**, 5579 (2000)
32. Y. Lifshitz, S.R. Kasi, J.W. Rabalais, Phys. Rev. Lett. **62**, 1290 (1989)
33. M.G. Fyta, I.N. Remediakis, P.C. Kelires, Phys. Rev. B **67**, 035423 (2003)
34. X. Chen, J. Narayan, J. Appl. Phys. **74**, 4168 (1993)
35. A.B. Anderson, J.J. Maloney, J. Phys. Chem. **92**, 809 (1988)